ISSN 0915-633X

NATIONAL INSTITUTE FOR FUSION SCIENCE

Bifurcation and Phase Diagram of Turbulence Constituted from Three Different Scale-length Modes

S.-I. Itoh, A. Kitazawa, M. Yagi and K. Itoh

(Received - 2002.3.13)

NIFS-726 Apr. 2002

RESEARCH REPORT
NIFS Series

TOKI, JAPAN

Bifurcation and phase diagram of turbulence constituted from three different scale-length modes

S.-I. Itoh[a], A. Kitazawa[a], M. Yagi[a] and K. Itoh[b]

[a] Research Institute for Applied Mechanics, Kyushu University, Kasuga 816-8580, Japan
[b]National Institute for Fusion Science, Toki, 509-5292, Japan

Abstract

Cases where three kinds of fluctuations having the different typical scale-lengths coexist are analyzed, and the statistical theory of strong turbulence in inhomogeneous plasmas is developed. Statistical nonlinear interactions between fluctuations are kept in the analysis as the renormalized drag, statistical noise and the averaged drive. The nonlinear interplay through them induces a quenching or suppressing effect, even if all the modes are unstable when they are analyzed independently. Variety in mode appearance takes place: one mode quenches the other two modes, or one mode is quenched by the other two modes, etc. The bifurcation of turbulence is analyzed and a phase diagram is drawn. Phase diagrams with cusp type catastrophe and butterfly type catastrophe are obtained. The subcritical bifurcation is possible to occur through the nonlinear interplay, even though each one is supercritical turbulence when analyzed independently. Analysis reveals that the nonlinear stability boundary (marginal point) and the amplitude of each mode may substantially shift from the conventional results of independent analyses.

Keywords: multiple scale-lengths, turbulence transition, strong turbulence, statistical theory, renormalization, subcritical bifurcation, phase diagram

1. INTRODUCTION

Recently, progress has been made in the field of theory and modelling of plasma turbulence. Methodologies of turbulence theories have been advanced, and the theory for turbulence suppression and transition is a successful example for it. (See, for a review, e.g. refs.[1-4].) In particular, emphasis has been made on the importance of the nonlinear interplay between separated fluctuations having the different typical scale lengths. The scale separation is often used in a conventional approach: one class of mode is analyzed independently where fluctuations of the other scale lengths are often neglected or given. It has been shown that this simplification is not always relevant, and the interactions between the modes with different scale lengths have a large impact on the evolution of the turbulence [5]. Other examples that show the importance of nonlinear interactions between different lengths include the dynamics of the meso-scale structure of the radial electric field and microscopic fluctuations [6], the electric field domain interface [7, 8], zonal flow [9, 10] and streamer [11].

Fluctuations in plasmas consist of different fluctuations with typical scale lengths being separated. For instance, fluctuations in the range of ion gororadius ($\sim \rho_i$) [12, 13] and those in the range of collisionless skin depth ($\sim c/\omega_p$) [14, 15] have been subject to an intensive experimental study. The longer wavelength mode has an important role for transport, even though the growth rate is small or negative [5]. As an opposite example, an importance of much-shorter wave-length fluctuations (e.g., the electron temperature gradient (ETG) mode with the scale length of electron gyroradius $\sim \rho_e$) is theoretically recognized [16]. These observations and studies clearly demonstrate the necessity of the study of the nonlinear interplay between fluctuations of different scale lengths.

In this paper, we analyze the turbulence composed of three different kinds of collective modes with different scale lengths. The nonlinear interplay is analyzed, and the transitions among them are investigated. A phase diagram is summarized. A new insight is given for the transition of turbulence. A butterfly type catastrophe as well as a cusp type catastrophe is revealed. A transition between different state of turbulence can be a subcritical excitation, even if each one might be excited through supercritical excitation when analyzed independently.

The constitution of this paper is the following. In section 2, the model and basic equations are given. Using a reduced set of equations for fluctuating fields, the self and mutual nonlinear interactions are formally divided into drags, drives and noises [5, 17-22]. A statistical average is made and a closed set of equations is given. An analysis on the turbulence bifurcation is given in section 3. The summary and discussion are given in section 4.

In order to discriminate three kinds of different scale lengths, we use the symbol

m, l, h

for the mode of the longest scale length, the intermediate scale length, and the shortest scale length, respectively. Names of 'macro', 'semi-micro', and 'micro' are also used in conjunction with this distinction of lengths. This choice of names only implies the order of lengths. When one analyzes the case of {ion temperature gradient (ITG) mode [3], current-diffusive interchange mode (CDIM) [23-25] and ETG mode}, the relevant lengths are ρ_i, c/ω_p and ρ_e. Then the name of 'macro mode' means the scale length of ρ_i, although this 'macro' mode has short wave length in comparison with the global scale lengths.

2. MODEL

2.1 Model equations and approximations

The derivation of statistical equation has been developed in previous articles [5, 18-22]. The dynamical equations of fluctuation fields are given in a form as

$$\frac{\partial}{\partial t} f + \mathcal{L}^{(0)} f = \mathcal{N}(f, f) + \tilde{S}_{th} \tag{1}$$

where $f^{\mathrm{T}} = \left(\phi, J_{\parallel}, V_{\parallel}, P_e, p_i\right)$ is the fluctuating component of electrostatic potential, parallel current, parallel velocity, electron pressure and ion pressure, and $\mathcal{N}(f, f)$ stands for the nonlinear terms $\mathcal{N}(f, f) = -\left(\nabla_{\perp}^{-2}\left[\phi, \nabla_{\perp}^2\phi\right], \left(1 - \xi\nabla_{\perp}^{-2}\right)^{-1}\left[\phi, J_{\parallel}\right], \left[\phi, V_{\parallel}\right], \left[\phi, P_e\right], \left[\phi, p_i\right]\right)$. The bracket $[f,g]$ denotes the Poisson bracket, $[f, g] = (\nabla f \times \nabla g)\cdot \boldsymbol{b}$, $\boldsymbol{b} = \boldsymbol{B}_0/B_0$ denotes the unit vector in the direction of the magnetic field and $\xi = \rho_i^2\delta^{-2}$. Physics variables (e.g., $\left(\phi, J_{\parallel}, V_{\parallel}, p_e, p_i\right)$, magnetic field B, electric field, length and time) are normalized according to a standard convention. Various choices of normalization are described in detail in ref.[26]. The linear operator $\mathcal{L}^{(0)}$ represents the linear property of fluctuations. $\mathcal{L}^{(0)}$ contains the influences of the plasma gradients (those of pressure, ion and electron temperatures), the transport coefficients by the collisional process (being expressed as $\mu_{\perp c}$, $\mu_{e,c}$, $\mu_{\parallel c}$, $\chi_{c,e}$, $\chi_{c,i}$ for the shear viscosity, electron viscosity, parallel viscosity of ions, electron thermal diffusivity and ion thermal diffusivity, respectively) the properties of the magnetic field (inhomogeneity, magnetic shear, etc.) or that of the radial electric field inhomogeneity.

The nonlinear terms are expressed as a sum of the drag, drive and the noise as

$$\mathcal{N}(f, f) = -\Gamma f + \mathcal{D} f + \tilde{S}_{\mathrm{self}} + \tilde{S}_{\mathrm{shorter}} \tag{2}$$

where $-\Gamma f$ is the drag term, $\mathcal{D} f$ is the drive term, $\tilde{S}_{\text{self}}$ is the self nonlinear noise term and $\tilde{S}_{\text{shorter}}$ is the nonlinear noise term owing to the fluctuations that belong to the class of much shorter scale lengths. The drag term is originated from the self drag and those by the fluctuations that belong to the class of shorter scale lengths. The drive term is owing to the fluctuations that belong to the class of much longer scale length. By use of Eq.(2), Langevin equations are derived from Eq.(1) as

$$\frac{\partial}{\partial t} f + \mathcal{L} f = \tilde{S}_{\text{self}} + \tilde{S}_{\text{shorter}} , \tag{3}$$

for macro, semi-micro and micro modes, respectively, where

$$\mathcal{L} = \mathcal{L}^{(0)} + \Gamma - \mathcal{D} \tag{4}$$

is the renormalized operator. A statistical modelling of the nonlinear term has been discussed in ref.[5]. In Appendix A, a brief summary is made.

The nonlinear dispersion relations are given as

$$\det\left(\lambda^m \boldsymbol{I} + \mathcal{L}^{(0)} + \Gamma^l_{(m)} + \Gamma^l_{(l)} + \Gamma^l_{(h)} \right) = 0 \tag{5a}$$

$$\det\left(\lambda^l \boldsymbol{I} + \mathcal{L}^{(0)} + \Gamma^l_{(l)} + \Gamma^l_{(h)} - \mathcal{D}^l_{(m)} \right) = 0 , \tag{5b}$$

$$\det\left(\lambda^h \boldsymbol{I} + \mathcal{L}^{(0)} + \Gamma^h_{(h)} - \mathcal{D}^h_{(m)} - \mathcal{D}^h_{(l)} \right) = 0 , \tag{5c}$$

where λ^m, λ^l and λ^h are nonlinear eigenvalues for the macro mode, semi-micro mode and micro mode, respectively. In the following, the index m, l and h stand for the macro, semi-micro and micro mode fluctuations, respectively.

2.2 Nonlinear equations for reduced variables

From the solution of the Langevin equations (3), a statistical average of fluctuation amplitude is derived. The Fluctuation Dissipation (FD) relation, that the average of fluctuation amplitude and noise satisfy, has been derived. With the help of diagonalization approximation, by which the correlation functions of noise terms are represented by the autocorrelation of fluctuations [18-22], one has an explicit form of the FD relation. The eddy-damping rate γ_j is related to the fluctuation amplitude through

renormalization relation. Equation (5), the FD relation and the renormalization relation for eddy damping rate [17] form a closed set of equations that determines the fluctuation levels (I^m , I^l , I^h), the decorrelation rates (λ^m , λ^l , λ^h) and the eddy-damping rates (γ_v^m , γ_v^l , γ_v^h) simultaneously in the presence of global inhomogeneities. A derivation has been discussed in [5] and is not repeated here. (See Appendices A and B.) A case of the combinations of {resistive-g mode, ion temperature gradient (ITG) mode and current-diffusive interchange mode (CDIM)} is explicitly explained also in the Appendix B. A set of equations which includes the nonlinear interplay between three classes of fluctuations is expressed for fluctuation amplitudes I^m , I^l and I^h [5]. Equations (B21)-(B23) form a closed set of reduced variables.

As is explained in the appendix, this set of equations for the fluctuation levels is characterized by several parameters. The controlling parameters are the driving source terms, $\left(D^m, D^l, D^h\right)$, and the critical levels of fluctuations for suppressing turbulence, $\left(I_{eff}^{l\leftarrow m}, I_{eff}^{h\leftarrow l}, I_{eff}^{h\leftarrow m}\right)$. They are defined as follows.

$$D^m = \left(1 + \left(\omega_E/\omega_{Ec}^m\right)^2\right)^{-1} \gamma_0^m \, k_0^{m-2} \,, \tag{6a}$$

$$D^l = \left(1 + \left(\omega_E/\omega_{Ec}^l\right)^2\right)^{-1} \gamma_0^l \, k_0^{l-2} \,, \tag{6b}$$

and

$$D^h = \left(1 + \left(\omega_{E1}/\omega_{Ec}^h\right)^2\right)^{-1} \gamma_0^h \, k_0^{h-2} \tag{6c}$$

represent driving sources for the macro, semi-micro and micro mode fluctuations, γ_0 stands for the each nonlinear growth rate without coupling and nonlinear noise, k_0^m , k_0^l and k_0^h are typical wavenumbers, and ω_{E1} is the $E \times B$ shearing rate by the global radial electric field,

$$\omega_{E1} = \frac{1}{B} \frac{d}{dr} E_r \,, \tag{7}$$

ω_{Ec}^m , ω_{Ec}^l and ω_{Ec}^h are the critical values for the suppression of the modes. The parameters

$$I_{eff}^{l\leftarrow m} \equiv \left(1 + \left(\omega_E/\omega_{Ec}^l\right)^2\right)\left(\omega_{Ec}^l\right)^2\left(k^m\right)^{-4} \tag{8a}$$

$$I_{eff}^{h\leftarrow l} \equiv \left(1+\left(\omega_E/\omega_{Ec}^h\right)^2\right)\left(\omega_{Ec}^h\right)^2\left(k^l\right)^{-4} \tag{8b}$$

and

$$I_{eff}^{h\leftarrow m} \equiv \left(1+\left(\omega_E/\omega_{Ec}^h\right)^2\right)\left(\omega_{Ec}^h\right)^2\left(k^m\right)^{-4} \tag{8c}$$

stand for the characteristic fluctuation level at which the semi-micro mode is suppressed by the macro mode, the micro mode by the semi-micro mode and the micro mode by the macro mode, respectively.

The coupled equations, which are shown as Eqs.(B21)-(B23) in Appendix B, are given in a normalized form for the macro, semi-micro and micro modes as

$$\left(1-x^2\right)^2 = \left(\frac{\hat{D}^l}{\hat{D}^m}\,\sigma\right)^2 \frac{1+\frac{x}{2}}{\left(1+\hat{D}^{m2}x^2\right)^2} \tag{9a}$$

$$y^2 = \left(\frac{\hat{D}^m}{\sigma\,\hat{D}^l}\right)^2\left(1-x^2\right)^2 - \frac{\hat{D}^h}{\hat{D}^l}\,\frac{\hat{D}^m}{\sigma\,\hat{D}^l}\left(1-x^2\right)z \tag{9b}$$

and

$$\left[z^2\left\{1+\left(\hat{D}^m\,\frac{\omega_{Ec}^l}{\omega_{Ec}^h}\right)^2 x^2+\left(\frac{\hat{D}^m}{\sigma}\right)^2\left(1-x^2\right)^2-\frac{\hat{D}^h\hat{D}^m}{\sigma}\left(1-x^2\right)z\right\}-1\right]^2$$

$$= \frac{x^2}{4}+\frac{1}{4}-\frac{\sigma\,\hat{D}^h}{4\hat{D}^m}\,\frac{z}{\left(1-x^2\right)}\,. \tag{9c}$$

In Eq.(9), a normalization is introduced for a convenience of the analysis. Levels of fluctuations are normalized as

$$x=\frac{\sqrt{I^m}}{D^m} \qquad y=\frac{\sqrt{I^l}}{D^l} \qquad z=\frac{\sqrt{I^h}}{D^h}\,. \tag{10}$$

As a unit of fluctuation level, one may use

$$\sqrt{I_{eff}^{h\leftarrow l}}=\frac{\omega_{Ec}^{h}}{\left(k^{l}\right)^{2}}\ ,\qquad \sqrt{I_{eff}^{h\leftarrow m}}=\frac{\omega_{Ec}^{h}}{\left(k^{m}\right)^{2}}\ \text{and}\ \sqrt{I_{eff}^{l\leftarrow m}}=\frac{\omega_{Ec}^{l}}{\left(k^{m}\right)^{2}} \tag{11}$$

We use normalized driving parameters as

$$\hat{D}^{h}=\frac{D^{h}}{\sqrt{I_{eff}^{h\leftarrow l}}}\ ,\qquad \hat{D}^{l}=\frac{D^{l}}{\sqrt{I_{eff}^{h\leftarrow l}}}\ \text{and}\ \hat{D}^{m}=\frac{D^{m}}{\sqrt{I_{eff}^{l\leftarrow m}}} \tag{12}$$

The driving parameters D^{h} and D^{l} are normalized to $\sqrt{I_{eff}^{h\leftarrow l}}$ which is the characteristic level of fluctuations for the semi-micro mode to suppress the micro mode. Additional parameter is introduced as

$$\sigma=\frac{\sqrt{I_{eff}^{h\leftarrow l}}}{\sqrt{I_{eff}^{l\leftarrow m}}}=\frac{\omega_{Ec}^{h}\left(k^{m}\right)^{2}}{\omega_{Ec}^{l}\left(k^{l}\right)^{2}}\ . \tag{13}$$

related to the normalization of D^{m} .

Equation (9) is derived for the condition that all the three classes of fluctuations are excited. If one amplitude out of them vanishes, the governing equations are reduced those for the two kinds of fluctuations and are given in [5].

3. Analysis of Bifurcation and Phase Diagram

A simplified analysis, in which nonlinear interactions between different fluctuations are neglected, gives an independent solutions

$$x=1\ ,\qquad y=1\ ,\ \text{and}\ z=1 \tag{14}$$

In the absence of the nonlinear interaction, three classes of fluctuations can be independently unstable and the levels are given by the solution

$$I^{m}\simeq\left(D^{m}\right)^{2}\ ,\ I^{l}\simeq\left(D^{l}\right)^{2}\ \text{and}\ I^{h}\simeq\left(D^{h}\right)^{2}\ . \tag{15}$$

Solutions of Eq.(9) give a new catastrophe structure with multiple solutions.

3.1 Overview of coupled equations

Before showing the detailed solutions of Eq.(9), a few remarks on an overview is made.

Equations (9a)-(9c) are nonlinear coupled equations of (x, y, z) for parameters $\hat{D}^m$, $\hat{D}^l$, $\hat{D}^h$, σ and $\omega_{Ec}^h/\omega_{Ec}^l$. This set of equations has the following characteristics. Variables y and z are eliminated form the equation for the macro mode, and Eq.(9a) is a closed equation for x. It is decoupled from Eqs.(9b) and (9c). The variable y is eliminated from the equation of the micro mode, and Eq.(9c) contains only x and z. From these properties, x is first solved from Eq.(9a). Once x is obtained, Eq (9c) is then solved, giving a solution of z. Substitution of solutions of x and z into Eq.(9b), y is solved immediately. The solution (x, y, z) is derived.

This set of equations (9) is deduced with the assumption that all the three modes have finite amplitude. In order that all the three kinds of fluctuations are excited,

$$x, y, z > 0 , \tag{16}$$

several constraints in the following are imposed. From Eq. (B21), x is bounded as

$$x < 1 . \tag{17}$$

This shows that the nonlinear coupling between semi-micro and micro modes always reduce the amplitude of the global mode. In the absence of the coupling, the solution $x = 1$ is given. From Eq.(9b), one finds a constraint

$$z < \frac{\hat{D}^m}{\sigma \hat{D}^h}\left(1 - x^2\right) . \tag{18a}$$

In addition, Eq.(9b) provides additional constraint that

$$y < \frac{\hat{D}^m}{\sigma \hat{D}^l}\left(1 - x^2\right) \tag{18b}$$

must be satisfied.

In the following subsections, the solutions (x, y, z) are shown for various ranges of driving parameters $\hat{D}^m$, $\hat{D}^l$ and $\hat{D}^h$. Number of solutions that satisfy Eq.(16) is investigated, and the phase diagram is drawn in the parameter space of $\hat{D}^m$, $\hat{D}^l$ and $\hat{D}^h$.

A care is necessary when one studies the relation between the set of equations (9) and the equations for the two kinds of modes which have been discussed in ref.[5]. When one studies the behaviour of the solution x, the analysis is given along a line similar to the one in ref.[5]. However, when one considers the solutions (y, z), the

situation is different. In the case that the macro mode is absent, Eq.(9a) is not required to be satisfied. One must use the simple result in ref.[5] for (y, z), and need not to proceed to Eq.(9). Equations (9a)-(9c) are deduced with the condition $0 < x, y, z$. The deduction of Eqs.(9a)-(9c) uses the relation $x > 0$, so that Eqs.(9b) and (9c) with $x = 0$ do not agree with the result in ref.[5]. In other words, the solution (x, y, z) does not always converge in the limit of $x \to 0$ to the solution (y, z) which is given in the theory of two kinds of fluctuations in ref.[5].

Keeping these characteristics in mind, the analysis of Eq.(9) is given in the following. First, the solution of the global mode is discussed in the subsection 3.2. Then the fluctuation amplitude of the semi-micro and micro modes are investigated in the subsection 3.3.

3.2 Excitation of the global mode

Equation (9a) is a closed equation for x, and studying it gives a perspective for the excitation of the global mode. Equation (9a) is rewritten as

$$\left(1-x^2\right)^2\left(1+\hat{D}^{m2}x^2\right)^2 = \left(\frac{\hat{D}^l}{\hat{D}^m}\sigma\right)^2\left(1+\frac{x}{2}\right). \tag{19}$$

The solution is controlled by two parameters, $\hat{D}^m$ and $\sigma\hat{D}^l/\hat{D}^m$, i.e., the magnitude of the drive of the macro mode and that of the semi-micro mode.

Equation (19) is solved for various values of controlling parameters. In the case that

$$\hat{D}^m < \hat{D}^m_{c,1} \simeq 1.29, \tag{20}$$

equation (19) can have one solution if the condition

$$\frac{\hat{D}^l}{\hat{D}^m}\sigma < 1 \tag{21}$$

is satisfied. Even for a fixed value of the self-driving parameter $\hat{D}^m$, the amplitude x is influenced by the coupling with the semi-micro mode. As is shown in Fig.1, x is a decreasing function of the drive of semi-micro mode $\sigma\hat{D}^l/\hat{D}^m$. At the critical value of

$$\frac{\hat{D}^l}{\hat{D}^m}\sigma = 1 \tag{22}$$

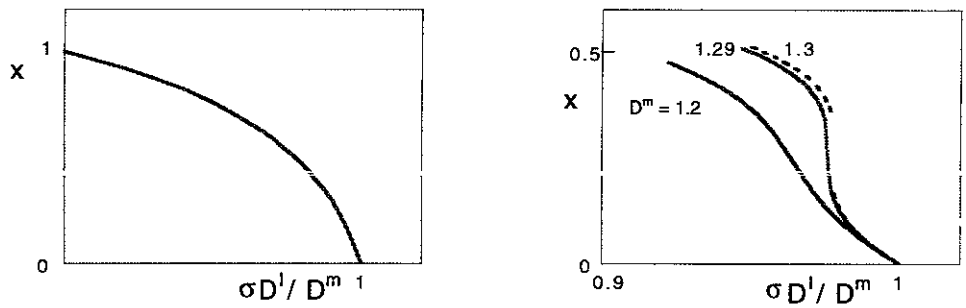

Fig.1. Amplitude of the macro mode x as a function of the drive of semi-micro mode $\sigma\hat{D}^l/\hat{D}^m$. The driving parameter $\hat{D}^m$ is fixed constant. An expanded view is given near the critical value of $\hat{D}^m \simeq \hat{D}^m_{c,1} \simeq 1.29$. Solid lines show the case of monotonous dependence on $\sigma\hat{D}^l/\hat{D}^m$, and dashed one indicates a cusp type bifurcation.

the macro mode is subject to the supercritical excitation.

When the driving parameter for the macro mode increases,

$$\hat{D}^m > \hat{D}^m_{c,1}\,, \tag{23}$$

multiple solutions can exist. As is illustrated in Fig.2, a cusp type catastrophe occurs. The branch of strong excitation of the macro mode (shown by the solid line) takes place in the parameter range

$$0 < \frac{\hat{D}^l}{\hat{D}^m}\sigma < c_1 \tag{24}$$

The lower branch of x appears near $\sigma\hat{D}^l/\hat{D}^m \simeq 1$ and disappears at $\sigma\hat{D}^l/\hat{D}^m = 1$, shown in an expanded view of Fig.1(b). In the parameter range of

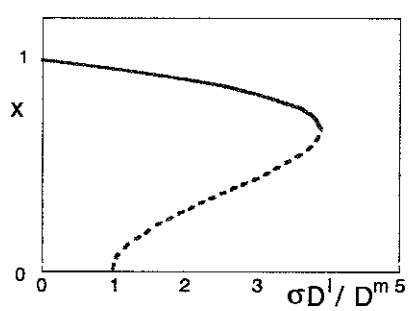

Fig.2. Amplitude of the macro mode x as a function of the drive of semi-micro mode $\sigma\hat{D}^l/\hat{D}^m$. The driving parameter $\hat{D}^m$ is fixed constant. Solid curve shows the branch of strongly excited macro turbulence. Dashed curve indicates an unstable branch.

$$c_2 < \frac{\hat{D}^l}{\hat{D}^m}\sigma < 1 \ , \tag{25}$$

three branches exist. Two are stable, and the intermediate one is unstable and is not realized as a stationary state. c_1 and c_2 denote the critical values and are functions of $\hat{D}^m$. $c_1\left(\hat{D}^m\right)$ and $c_2\left(\hat{D}^m\right)$ are estimated later. In the range of

$$1 < \frac{\hat{D}^l}{\hat{D}^m}\sigma < c_1 \ , \tag{26}$$

the lower branch disappears (i.e., only being sustained by noise). It should be noted that the subcritical excitation takes place at the critical condition

$$\sigma\hat{D}^l/\hat{D}^m = c_1 \ . \tag{27}$$

This subcriticality is owing to the nonlinear interaction with semi-micro and micro fluctuations. Even though the drive of the macro mode $\hat{D}^m$ is positive, the macro mode can be quenched.

The boundaries $c_1\left(\hat{D}^m\right)$ and $c_2\left(\hat{D}^m\right)$ are analytically estimated. In the limit of large $\hat{D}^m$, the left hand side of Eq.(19) takes maximum value

$$f_{\mathrm{m}} \equiv \frac{\left(1+\hat{D}^{m2}\right)^4}{16\hat{D}^{m4}} \qquad \text{at} \qquad x = x_{\mathrm{m}} = \sqrt{\frac{1}{2} - \frac{1}{2}\hat{D}^{m-2}} \tag{28}$$

A critical condition of the ridge point of Fig.2 is estimated by the condition that the right hand side is equal to f_{m} at $x = x_{\mathrm{m}}$, i.e.,

$$\frac{\hat{D}^l}{\hat{D}^m}\sigma = c_1 = \frac{\left(1+\hat{D}^{m2}\right)^2}{4\hat{D}^{m2}}\left(\frac{2\sqrt{2}}{2\sqrt{2}+\sqrt{1-\hat{D}^{m-2}}}\right)^{1/2} . \tag{29}$$

Expanding the left hand side of Eq.(19) up to the quadratic term, the lower boundary c_2 for the critical condition is estimated as

$$\frac{\hat{D}^l}{\hat{D}^m}\sigma = c_2 = \left(1 - \frac{1}{32}\frac{1}{\hat{D}^{m2}-1}\right)^{1/2} . \tag{30}$$

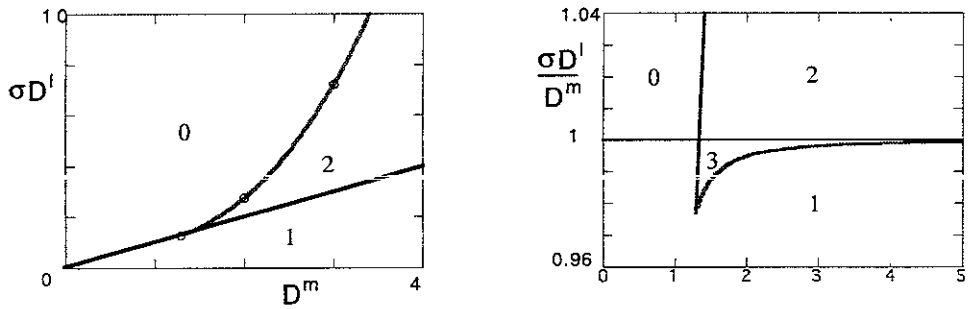

Fig.3 Phase diagram for the macro fluctuations in the parameter space of ($\hat{D}^m$, $\sigma\hat{D}^l$). (a) Numbers in the segmented regions denote the number of solutions of x . A solid curve is an analytic estimate and circles show numerical solutions. An expanded view is given in (b) on ($\hat{D}^m$, $\sigma\hat{D}^l/\hat{D}^m$) plane.

The phase diagram is shown in Fig.3(a) in the parameter space of $\left(\hat{D}^m, \sigma\hat{D}^l\right)$. Numbers in the segmented regions denote the number of solutions of x . A solid curve in Fig.3(a) is an analytic estimate Eq.(29) and circles show numerical solutions. An expanded view is given in Fig.3(b) on the $\left(\hat{D}^m, \sigma\hat{D}^l/\hat{D}^m\right)$ plane.

3.3 Excitation of the semi-micro and micro modes

3.3.1 Case of weak drive for macro mode

When the drive for the macro mode is weak and the parameter $\hat{D}^m$ is small, $\hat{D}^m << 1$, x has only one solution in the range of Eq.(21). Amplitudes y and z are given as a function of $\hat{D}^l$ and $\hat{D}^h$. (When Eq.(21) is not satisfied, the macro mode is quenched. The problem reduces to the one for nonlinear interaction between two kinds of fluctuations, and has been analyzed in [5], and is not reproduced in this article.)

Figure 4 illustrates the amplitudes y and z as a function of the driving parameter $\hat{D}^l$ for a fixed value of $\hat{D}^h$. (Examples of the parameters are chosen as $\omega_{Ec}^h/\omega_{Ec}^l = 2$, $\left(k^m/k^l\right)^2 = 1/10$ and $\sigma = 1/5$.) When the driving source of the semi-micro mode is weak, $\hat{D}^l << 1$, the fluctuation is dominated by the global mode, x . The other scale fluctuations are suppressed by the global mode. As the drive of the semi-micro mode $\hat{D}^l$ increases, one branch of fluctuations $\left(y_1, z_1\right)$ (weak semi-micro mode and strong micro mode) appears. The behavior near the critical point is the supercritical excitation for the semi-micro mode. (The critical condition for excitation of the semi-micro mode is shifted from $\hat{D}^l = 0$ to a finite value of $\hat{D}^l$, owing to the presence of the macro mode fluctuations.) There are two states of fluctuations in which all the three modes are excited simultaneously. With the increase of the drive for semi-micro mode, the second state of the fluctuations $\left(y_2, z_2\right)$ is allowed to appear. The amplitude of z_2 exceeds unity, that is,

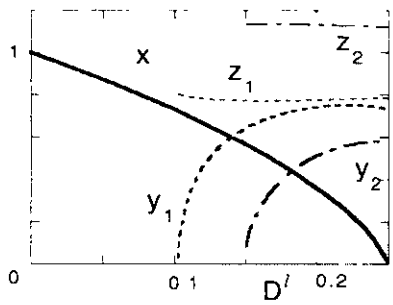

Fig.4 Amplitudes of the macro mode, semi-micro and micro mode fluctuations as a function of the drive of the semi-micro mode $\hat{D}^l$. Other parameters are fixed as $\hat{D}^m = 1/20$, $\hat{D}^h = 0.15$ and $\sigma = 1/5$. (Thick solid curve shows x . Dotted curves for one solution (x, y_1, z_1), and dashed-dotted curves for the other solution (x, y_2, z_2). Thick curves for y and thin ones for z .)

the micro mode (z_2) is more strongly excited than the case where this mode is independently excited. When $\hat{D}^l$ further increases, the macro mode is quenched by the semi-micro and micro mode. The state, in which all three fluctuations are strongly excited, disappears.

Based on the study of solutions, a phase diagram is drawn. The phase diagram is illustrated in Fig.5 on the $\left(\hat{D}^l, \hat{D}^h\right)$ plane. Number in the phase diagram indicates the numbers of states in which all of macro, semi-micro and micro fluctuations are strongly excited. (Figure 4 illustrates the solutions one the disection at $\hat{D}^h = 0.15$.) In the upper-left region of Fig.5, the semi-micro and micro modes are suppressed. In the right-end region, the macro mode is quenched. In an intermediate region, all the macro, semi-micro and micro mode fluctuations are excited strongly. The boundary between "1" and "2" in Fig.5 is estimated in the small $\hat{D}^m$. This boundary is given by the condition $y = 0$. This yields $z = \hat{D}^m\left(1 - x^2\right)/\sigma\hat{D}^h$. Substitution of this into Eq.(9c) provides the

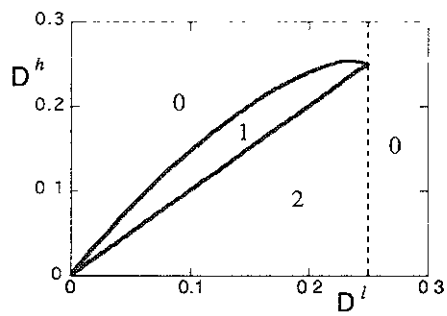

Fig.5 Phase diagram on the ($\hat{D}^l$, $\hat{D}^h$) plane. Other parameters are fixed as $\hat{D}^m = 1/20$ and $\sigma = 1/5$.

relation $\left(1-x^2\right)^2 / \left\{1+\left(\hat{D}^m\,\omega_{Ec}^l/\omega_{Ec}^h\right)^2 x^2\right\} = \left(\sigma\hat{D}^h/\hat{D}^m\right)^2\left(1\pm\frac{x}{2}\right)$. Elimination of x from this equation and Eq.(9a) provides the boundaries, giving

$$\hat{D}^l \simeq \hat{D}^h \ . \tag{31}$$

3.3.2 Case of intermediate drive for macro mode

When the drive for the macro mode is moderate and the parameter $\hat{D}^m$ takes an intermediate value, $\hat{D}^m \simeq 1$, more complicated behaviour appears although x has only one solution in the range of Eq.(21). Amplitudes y and z are given by solving Eq.(9).

Figure 6 illustrates the amplitudes x, y and z as a function of the driving parameter $\hat{D}^l$ for a fixed value of $\hat{D}^h$. (Examples of the parameters are chosen as $\hat{D}^m \simeq 1$, $\omega_{Ec}^h/\omega_{Ec}^l = 2$, $\left(k^m/k^l\right)^2 = 1/10$ and $\sigma = 1/5$.) In this figure, the thick solid curve indicates x. The semi-micro mode is denoted by thick dashed curve and thick dotted-dashed curve. The micro mode is expressed by thin dashed curve and thin dotted-dashed curve. (The dotted curves indicate a solution $\left(x, y_1, z_1\right)$, and dotted-dashed curves show another solution $\left(x, y_2, z_2\right)$, respectively.) When the driving source of the semi-micro mode is weak, the global mode suppresses other modes. When $\hat{D}^l$ increases, one branch of fluctuations, in which both the semi-micro and micro mode fluctuations are subcritically excited near the critical point together with macro mode, appears. At this critical point, two branches of fluctuation states appear. The nonlinear interplay induces the subcritical excitation of semi-micro and micro mode fluctuations. As the drive for semi-micro mode increases, the second bifurcation takes place, and the third and fourth of the fluctuation states are allowed. (The solutions $\left(x, y_1, z_1\right)$ and $\left(x, y_2, z_2\right)$ are multiple valued. In one solution of $\left(x, y_1, z_1\right)$ or $\left(x, y_2, z_2\right)$, the pair of a larger value of y and a smaller one of z (or vice versa) represents the solution.) When $\hat{D}^l$ further increases, the macro mode is quenched by the other two modes.

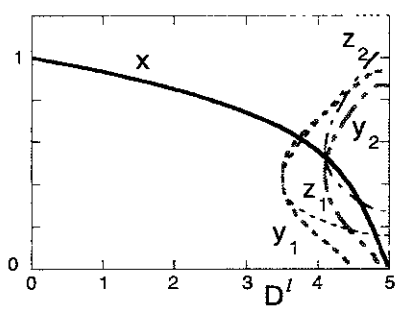

Fig.6 Amplitudes of the macro mode, semi-micro and micro mode fluctuations as a function of the drive of the semi-micro mode $\hat{D}^l$. Other parameters are fixed as $\hat{D}^m = 1$, $\hat{D}^h = 4.8$ and $\sigma = 1/5$. (Dotted curves for one solution (x, y_1, z_1), and dashed-dotted curves for another solution (x, y_2, z_2). Thick curves for y and thin ones for z .)

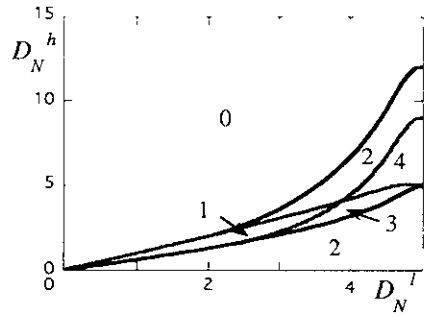

Fig.7 Phase diagram of turbulent state on the plane of normalized parameters $D_N^l = D^l/\sqrt{I_{eff}^{h\leftarrow l}}$ and $D_N^h = D^h/\sqrt{I_{eff}^{h\leftarrow l}}$. D^m is fixed as $D^m = (1/5)\sqrt{I_{eff}^{h\leftarrow l}}$. Numbers in the diagram denote the possible numbers of branches in which all the three components are simultaneously excited.

Figure 7 illustrates the phase diagram on the $(\hat{D}^l, \hat{D}^h)$ plane. It contains a butterfly catastrophe that governs the state of fluctuations. There appear three critical points which are shown in Fig.7. Figure 6 shows the solutions on the disection of figure 7 at $\hat{D}^h = 4.8$. This new catastrophe is induced by the nonlinear interactions among three different classes of fluctuations.

3.3.3 Case of strong drive of macro mode

When the drive for the macro mode is so strong that Eq.(23) is satisfied, the amplitude of the global mode is subject to the cusp catastrophe. There are two branches of the macro-mode fluctuations: the branches of Eq.(24) and (26). ('upper' and 'lower' branches, respectively.) For each solution x , solutions of y and z are obtained, which are subject to a multiple bifurcation. Complex type of bifurcation is obtained.

Figure 8 illustrates the amplitudes x, y and z as a function of the driving parameter $\hat{D}^l$ for an intermediate value of $\hat{D}^h$. (Parameters are chosen as $\hat{D}^m = 3$, $\omega_{Ec}^h/\omega_{Ec}^l = 2$, $(k^m/k^l)^2 = 1/10$, $\sigma = 1/5$ and $\hat{D}^h = 5$.) Figure 8(a) shows the solution associated with the upper branch of x, and figure 8(b) is for the lower branch of x. (As in Fig.6, dotted curves are for one solution (x, y_1, z_1), and the dashed-dotted curves are for another solution (x, y_2, z_2). Thick curves denote y and thin curves indicate z.)

First, the solution associated with the upper-branch of x is investigated. (Figure 8(a)) When $\hat{D}^l$ is small, the other scale fluctuations are suppressed by the global mode. As $\hat{D}^l$ increases, one branch of fluctuations with three modes appears as the supercritical excitation. With the increase of $\hat{D}^l$, the second bifurcation takes place, which can be also the subcritical excitation. The amplitudes of semi-micro and micro modes can have comparable magnitudes in this region (for both (y_1, z_1) and (y_2, z_2)). When $\hat{D}^l$ further increases, the macro mode is quenched by the other two.

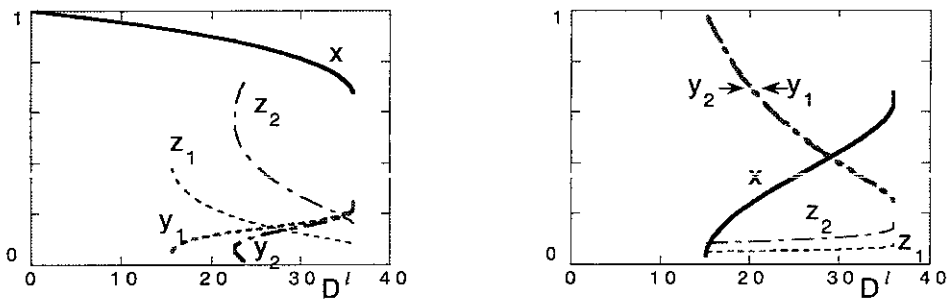

Fig.8 Amplitudes of the macro, semi-micro and micro mode fluctuations as a function of $\hat{D}^l$. $\hat{D}^m$, $\hat{D}^h$ and σ, are fixed as $\hat{D}^m = 3$, $\hat{D}^h = 5$ and $\sigma = 1/5$. The upper branch of x (a), and the lower branch of x (b). (Dotted curves for one solution (x, y_1, z_1), and dashed-dotted curve for another solution (x, y_2, z_2). Thick curves for y and thin curves for z.)

Next, the lower-branch of x is investigated. (Figure 8(b).) This branch does not exist except in an intermediate range of $\hat{D}^l$ in which Eq.(26) is satisfied. There are two solutions of (y, z) for this lower branch of x. In this case, the semi-micro mode is most strongly excited than others, whose amplitude can exceeds unity.

Figure 9 illustrates the amplitudes x, y and z as a function of $\hat{D}^l$ for a large value of $\hat{D}^m$. (Parameters are chosen as $\hat{D}^m = 3$, $\omega_{Ec}^h/\omega_{Ec}^l = 2$, $\left(k^m/k^l\right)^2 = 1/10$, $\sigma = 1/5$ and $\hat{D}^h = 12$.) Figure 9(a) and (b) show the solutions associated with the upper and lower branches of x, respectively. Correspondence of curves is the same as in Fig.8. For the upper-branch of x, the features of solutions (x, y_1, z_1) and (x, y_2, z_2) are similar to the case in Fig.8(a), except that the solution (x, y_1, z_1) appears via subcritical excitation. Features of solutions of the lower branch of x in Fig.9(b) are similar to those in Fig.8(b).

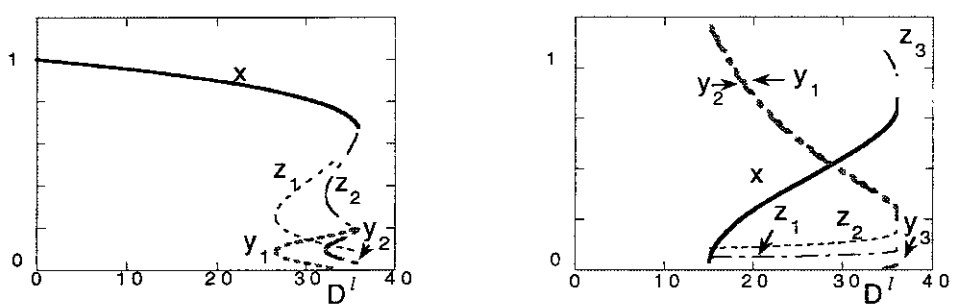

Fig.9 Amplitudes of the macro, semi-micro and micro mode fluctuations as a function of $\hat{D}^l$. $\hat{D}^m$, $\hat{D}^h$ and σ, are fixed as $\hat{D}^m = 3$, $\hat{D}^h = 12$ and $\sigma = 1/5$. The upper branch of x (a), and the lower branch of x (b). (Dotted curves for one solution (x, y_1, z_1), and dashed-dotted curve for another solution (x, y_2, z_2). Thick curves for y and thin curves for z.)

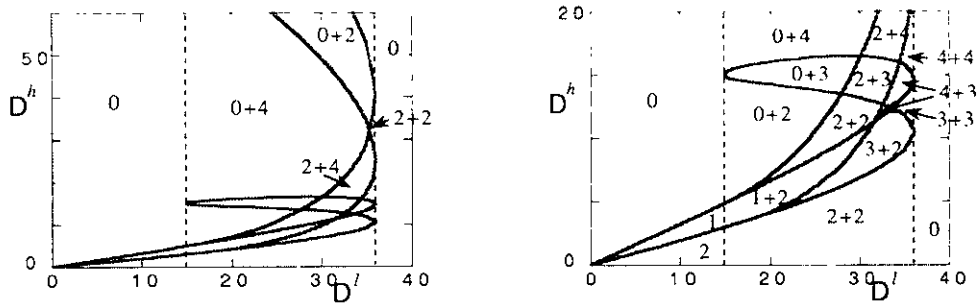

Fig.10 Phase diagram on the $(\hat{D}^l, \hat{D}^h)$ plane. Other parameters are fixed as $\hat{D}^m = 3$ and $\sigma = 1/5$. Expanded view in given in (b).

Summarizing these studies of solutions, the phase diagram is given in Fig.10. Where the number '0' is written, one or two kinds of modes are quenched. In Fig.10, 'i'+'j' means that there are number of i solutions belong to the upper branch of x and j solutions to the lower branch of x.

4. Summary and Discussion

In this paper, we have analyzed the turbulence composed of three kinds of collective modes with different scale lengths. A new insight was given for the transition of turbulence. The nonlinear interplay between them was analyzed, and various kinds of turbulent states were found. The transitions among turbulent states were investigated. A phase diagram was summarized. A butterfly type catastrophe as well as a cusp type catastrophe were revealed. It is stressed that the condition for the appearance of one kind of fluctuations with one characteristic scale length is strongly influenced by the presence of other kinds of fluctuations. One is quenched by the others, or one suppresses the others. The level of macro mode is always reduced by the nonlinear coupling, i.e. $x < 1$, for the simultaneous existence of the three modes. However, the semi-micro or the micro mode can extra-excited by the others over its own level, i.e., $y > 1$ or $z > 1$. Due to this, a prediction of the critical condition for the onset of fluctuations deviates considerably from the one which is derived by linear stability analysis. A transition between different state of turbulence could be a subcritical excitation, even if each one might be excited through supercritical excitation when analyzed independently.

Other important issue is the presence of the intermediate states. As is shown by the phase diagrams, there are many states, for a given set of driving parameters $\left(\hat{D}^m, \hat{D}^l, \hat{D}^h\right)$, with different amplitudes of meso-scale and micro scale fluctuations. These are called intermediate states. A statistical average of turbulence level and accessibility to a particular state of turbulence from other states are strongly influenced by the appearance of the intermediate states. A statistical analysis that describes the

dynamics between different states of turbulence must be investigated, and is left for future study.

We have analyses the nonlinear interplay between three kinds of modes in turbulent plasmas. The basic mechanisms of these nonlinear interactions are generic. The subcritical excitation owing to the presence of fluctuations of other scale length can be applied to the sudden appearance of the "events" or "collapse phenomena", such as sawtooth activities etc [27]. Furthermore, the basic concept can be used for the systems of complexity, which requires the further study.

Acknowledgements

Authors wish to acknowledge Prof. A. Fukuyama and Prof. A. Yoshizawa for useful discussions. This work is partly supported by the Grant-in-Aid for Scientific Research of Ministry of Education, Culture, Sports, Science and Technology (MEXT) Japan, by the collaboration programme of National Institute for Fusion Science and by the collaboration programme of the Research Institute for Applied Mechanics of Kyushu University.

Dedication:

This article is dedicated to Prof. A. Yoshizawa on occasion of the 60th anniversary of his birth.

Appendix A: Statistical modelling

A statistical modelling of the nonlinear term has been discussed in ref.[5]. In this appendix A, a brief summary is made.

The renormalized drag (coherent part) is given in a form of the eddy-viscosity type nonlinear transfer rate γ_j. A random-noise part is regarded to have a shorter decorrelation time than γ_j^{-1} according to rapid change model [17]. The nonlinear drag term is written in an apparent linear term as

$$\left(\Gamma f\right)^{\mathrm{T}}=\left(\gamma_1 f_1, \gamma_2 f_2, \gamma_3 f_3, \gamma_4 f_4, \gamma_5 f_5\right) \quad . \tag{A1}$$

We employ the expression that the superscripts m , l and h denote the macro, semi-micro and micro modes, respectively, and the subscripts (m) , (l) and (h) denote the contributions from the macro, semi-micro and micro modes, respectively. The driving part in the nonlinear interactions is deduced, giving

$$\mathcal{D}^h{}_{j,j}=\mathcal{D}^h_{(m)j,j}+\mathcal{D}^h_{(l)j,j}=-i\,\omega_{E(m)}-i\,\omega_{E(l)} \tag{A2a}$$

$$\mathcal{D}^l{}_{j,j}=\mathcal{D}^l_{(m)j,j}=-i\,\omega_{E(m)} \tag{A2b}$$

($j=1$, $j=3-5$),

$$\mathcal{D}^h{}_{2,2}=\mathcal{D}^h_{(m)2,2}+\mathcal{D}^h_{(l)2,2}=-i\,\xi^{-1}\omega_{E(m)}-i\,\xi^{-1}\omega_{E(l)} \tag{A2c}$$

$$\mathcal{D}^l_{(m)2,2}=-i\,\xi^{-1}\omega_{E(m)}\,, \tag{A2d}$$

$$\mathcal{D}^h{}_{j,1}=\mathcal{D}^h_{(m)j,1}+\mathcal{D}^h_{(l)j,1}=-i\,\omega_{j(m)}-i\,\omega_{j(l)} \tag{A2e}$$

$$\mathcal{D}^l_{(m)j,1}=-i\,\omega_{j(m)} \tag{A2f}$$

($j=3-5$) and

$$\mathcal{D}^h{}_{2,1}=\mathcal{D}^h_{(m)2,1}+\mathcal{D}^h_{(l)2,1}=-i\,\xi^{-1}\,\omega_{2(m)}-i\,\xi^{-1}\,\omega_{2(l)} \tag{A2h}$$

$$\mathcal{D}^l_{(m)2,1}=-i\,\xi^{-1}\,\omega_{2(m)}\,, \tag{A2i}$$

where

$$\omega_{E(m)} = k_y \frac{\partial}{\partial x}\tilde{\phi}^m - k_x \frac{\partial}{\partial y}\tilde{\phi}^m \quad \text{and} \quad \omega_{E(l)} = k_y \frac{\partial}{\partial x}\tilde{\phi}^l - k_x \frac{\partial}{\partial y}\tilde{\phi}^l \tag{A3a}$$

are the Doppler shifts owing to the $E \times B$ velocity associated with the macro mode and semi-micro mode, and

$$\omega_{j(m)} = -k_y \frac{\partial}{\partial x}\tilde{f}_j^m + k_x \frac{\partial}{\partial y}\tilde{f}_j^m \quad \text{and} \quad \omega_{j(l)} = -k_y \frac{\partial}{\partial x}\tilde{f}_j^l + k_x \frac{\partial}{\partial y}\tilde{f}_j^l \tag{A3b}$$

($j = 2-5$) represent the modification of plasma parameter by the macro mode and semi-micro mode, respectively.

Appendix B: An example of coupled equations

In this appendix, a case study for the combinations of {resistive-g mode, ITG mode and CDIM} is explicitly shown.

B1. Nonlinear eigenvalue

B1.1 Macro mode

Nonlinear growth rate of the mode is given as

$$\gamma_0^m = \left(\frac{G_0 \gamma_\chi^{m2}}{\gamma_v^m} \right)^{1/3} \exp\left(-\frac{\pi s}{2} \sqrt{\frac{\gamma_\chi^m}{G_0 \eta k_\theta^{m2}}} \right), \tag{B1}$$

where η is the resistivity, G_0 is the normalized pressure gradient coupled with the gradient of the magnetic field

$$G_0 = \nabla \ln p_0 \cdot \nabla \ln B_0 , \tag{B2}$$

μ_v is the ion viscosity, $\gamma_v^m = \mu_v k_0^{m2}$ is the eddy damping rate, and $\gamma_\chi^m = \chi k_0^{m2}$. If the thermal conductivity has the similar value to that of the ion shear viscosity, $\mu_v \simeq \chi$, the renormalized growth rate is approximated as

$$\gamma_0^m = \left(G_0 \gamma_v^m \right)^{1/3} \exp\left(-\frac{\pi s}{2} \sqrt{\frac{\gamma_v^m}{G_0 \eta k_\theta^{m2}}} \right). \tag{B3}$$

The nonlinear eigenvalue is given as

$$\Re e \lambda^m = -\left(1 + \left(\omega_{E1} / \omega_{Ec}^m \right)^2 \right)^{-1} \gamma_0^m + \gamma_v^m . \tag{B4}$$

B1.2 Semi-micro mode

The growth rate has been calculated as [3]

$$\gamma_0^l = \frac{r}{qR} s \left(1 + \eta_i \right) \left| \omega_{*i} \right| , \tag{B5}$$

and the critical value of the $E \times B$ shearing rate was given as

$$\omega_{Ec}^l \equiv \left(2 / \sqrt{1 + \eta_i} \right) \gamma_0^l . \tag{B6}$$

The shearing rate by the macro mode on the semi-micro mode has been given as [5]

$$\left|\omega_{E(m)}\right| = \left(k^m\right)^2 \sqrt{I^m} \ . \tag{B7}$$

The nonlinear eigenvalue is expressed as

$$\Re\mathrm{e}\,\lambda^l = -\frac{\gamma_0^l \sqrt{1 + \left|k_0^{m2}/2\gamma_v^m\right| \sqrt{I^m}}}{1 + \left(\omega_{E1}/\omega_{Ec}^l\right)^2 + \left(k^m\right)^4 \left(\omega_{Ec}^l\right)^{-2} I^m} + \gamma_v^l \ . \tag{B8}$$

B1.3 Micro mode

The nonlinear growth rate has been calculated as [23]

$$\gamma_0^h = \sqrt{G_0}\, v_A / qR \tag{B9}$$

and the critical value of the $E \times B$ shearing rate was given as [28]

$$\omega_{Ec}^h \simeq s\, v_{thi} / \sqrt{aR} \ . \tag{B10}$$

The shearing rates by the macro mode and the semi-micro are given as [5]

$$\left|\omega_{E(l)}\right| = \left(k^l\right)^2 \sqrt{I^l} \ , \tag{B11}$$

and

$$\left|\omega_{E(m)}\right| = \left(k^m\right)^2 \sqrt{I^m} \ . \tag{B12}$$

The nonlinear eigenvalue is expressed as

$$\Re\mathrm{e}\,\lambda^h = -\frac{\gamma_0^h \sqrt{1 + \sqrt{\left(k_0^{l\,2}/2\gamma_v^l\right)^2 I^l + \left(k_0^{m2}/2\gamma_v^m\right)^2 I^m}}}{1 + \left(\omega_{E1}/\omega_{Ec}^h\right)^2 + \left(k^l\right)^4 \left(\omega_{Ec}^h\right)^{-2} I^l + \left(k^m\right)^4 \left(\omega_{Ec}^h\right)^{-2} I^m} + \gamma_v^h \ . \tag{B13}$$

B2. Equation for stationary states

Conditions for stationary state are given for macro, semi-micro and micro mode as

$$\left(1 + \left(\omega_{E1}/\omega_{Ec}^m\right)^2\right)^{-1} \gamma_0^m - \gamma_v^m = 0 \ , \qquad \text{(macro)} \tag{B14}$$

$$\frac{\gamma_0^l\sqrt{1+\left|k_0^{m2}/2\gamma_v^m\right|\sqrt{I^m}}}{1+\left(\omega_{E1}/\omega_{Ec}^l\right)^2+\left(k^m\right)^4\left(\omega_{Ec}^l\right)^{-2}I^m}-\gamma_v^l=0\ , \qquad \text{(semi-micro)} \quad \text{(B15)}$$

and

$$\frac{\gamma_0^h\sqrt{1+\sqrt{\left(k_0^{l2}/2\gamma_v^l\right)^2I^l+\left(k_0^{m2}/2\gamma_v^m\right)^2I^m}}}{1+\left(\omega_{E1}/\omega_{Ec}^h\right)^2+\left(k^l\right)^4\left(\omega_{Ec}^h\right)^{-2}I^l+\left(k^m\right)^4\left(\omega_{Ec}^h\right)^{-2}I^m}-\gamma_v^h=0\ , \quad \text{(micro)} \qquad \text{(B16)}$$

respectively.

Eddy damping rate is expressed in terms of the fluctuation amplitude. The eddy damping rate for the macro mode is given as

$$\frac{\gamma_v^{l\,2}}{\left(k_0^l\right)^4}\simeq I^m+\frac{\gamma_v^m}{\left(k_0^l\right)^2}\frac{\gamma_v^l}{\left(k_0^l\right)^2} \qquad \text{(B17a)}$$

or

$$\frac{\gamma_v^m}{\left(k_0^m\right)^2}\simeq\frac{1}{2}\left(\frac{\gamma_v^l}{\left(k_0^l\right)^2}+\sqrt{\frac{\left(\gamma_v^l\right)^2}{\left(k_0^l\right)^4}+4I^m}\right). \qquad \text{(B17b)}$$

For semi-micro mode one has

$$\gamma_v^{l\,2}\simeq\left(k_0^l\right)^4I^l+\left(k_0^l\right)^2\left(k_0^h\right)^2\left(\gamma_v^l/\gamma_v^h\right)I^h \qquad \text{(B18)}$$

that is

$$\frac{\gamma_v^{l\,2}}{k_0^{l\,4}}\simeq I^l+\frac{\gamma_v^l}{k_0^{l\,2}}\sqrt{I^h} \qquad \text{(B19a)}$$

or

$$\frac{\gamma_v^l}{k_0^{l\,2}}\simeq\frac{1}{2}\left(\sqrt{I^h}+\sqrt{I^h+4I^l}\right). \qquad \text{(B19b)}$$

The eddy damping rate for the micro mode is given as

$$\gamma_v^h \simeq k_0^{h2}\sqrt{I^h} \ . \tag{B20}$$

B3. Coupled nonlinear equations

Equations (B14), (B15), (B16), (B17b), (B19b) and (B20) form a set of coupled equations for the eddy damping rates γ_v^m, γ_v^l, γ_v^h and the spectral functions I^m, I^l, I^h for given set of plasma parameters. Elimination of the eddy damping rates γ_v^m , γ_v^l and γ_v^h from Eqs.(B14), (B15), (B16), (B17b), (B19b), (B20), gives a final set of closed equations for I^m , I^l and I^h as

$$\frac{1}{4}\left(\sqrt{I^h}+\sqrt{I^h+4I^l}+\sqrt{\left(\sqrt{I^h}+\sqrt{I^h+4I^l}\right)^2+16I^m}\right)=D^m \tag{B21}$$

$$\frac{1}{2}\left(\sqrt{I^h}+\sqrt{I^h+4I^l}\right)=D^l\frac{\sqrt{1+\sqrt{I^m}/2D^m}}{\left(1+I^m I_{eff}^{l\leftarrow m-1}\right)} \tag{B22}$$

and

$$\frac{I^h}{\left(D^h\right)^2}=\frac{1+\sqrt{\dfrac{I^m}{4D^{m2}}+\dfrac{I^l}{4D^{l2}}\dfrac{\left(1+I^m I_{eff}^{l\leftarrow m-1}\right)^2}{\left(1+\sqrt{I^m}/2D^m\right)}}}{1+I_{eff}^{h\leftarrow l-1}I^l+I_{eff}^{h\leftarrow m-1}I^m} \ , \tag{B23}$$

where

$$D^m=\left(1+\left(\omega_E/\omega_{Ec}^m\right)^2\right)^{-1}\gamma_0^m\,k_0^{m-2} \ , \tag{B24a}$$

$$D^l=\left(1+\left(\omega_E/\omega_{Ec}^l\right)^2\right)^{-1}\gamma_0^l\,k_0^{l-2} \ , \tag{B24b}$$

and

$$D^h=\left(1+\left(\omega_{E1}/\omega_{Ec}^h\right)^2\right)^{-1}\gamma_0^h\,k_0^{h-2} \tag{B24c}$$

represent driving sources for the macro, semi-micro and micro mode fluctuations, respectively. The parameters

$$I_{eff}^{l\leftarrow m} \equiv \left(1 + \left(\omega_E/\omega_{Ec}^{l}\right)^2\right)\left(\omega_{Ec}^{l}\right)^2\left(k^m\right)^{-4} \tag{8a}$$

$$I_{eff}^{h\leftarrow l} \equiv \left(1 + \left(\omega_E/\omega_{Ec}^{h}\right)^2\right)\left(\omega_{Ec}^{h}\right)^2\left(k^l\right)^{-4} \tag{8b}$$

and

$$I_{eff}^{h\leftarrow m} \equiv \left(1 + \left(\omega_E/\omega_{Ec}^{h}\right)^2\right)\left(\omega_{Ec}^{h}\right)^2\left(k^m\right)^{-4} \tag{8c}$$

represents the critical level for suppression.

REFERENCE

[1] Yoshizawa A, Itoh S-I, Itoh K, Yokoi N: Plasma Phys. Control. Fusion **43** (2001) R1.
[2] Connor J W: Plasma Phys. Contr. Fusion **30** (1988) 619.
[3] Horton C W: Rev. Mod. Phys. **71** (1999) 735.
[4] Krommes J A: "Fundamental statistical theories of plasma turbulence in magnetic fields" Phys. Reports in press (2002).
[5] Itoh S-I and Itoh K: Plasma Phys. Contr. Fusion **43** (2001) 1055.
[6] Itoh K, Itoh S-I and Fukuyama A: *Transport and Structural Formation in Plasmas* (IOP, Bristol, 1999)
[7] Itoh S-I, Itoh K, Fukuyama A and Miura Y : *Phys. Rev. Lett.* **67** (1991) 2485.
[8] Diamond P H, Lebedev V B, Newman D E, Carreras B A, Hahm T S, Tang W M, Rewoldt G and Avinash K: Phys. Rev. Lett. **78** (1997) 1472.
[9] Smolyakov A I and Diamond P H: Phys. Plasmas **6** (1999) 4410.
[10] Krommes J A and Kim C-B: Phys. Rev. E. **62** (2000) 8508.
[11] Drake J F, Zeiler A, Biskamp D: Phys. Rev. Lett. **75** (1995) 4222.
[12] Fonck R J, Durst R, Evensen H, Kim J S, Bretz N L, Mazzucato E, Nazikian R, Paul S F, Lee W W, Levinton F M, et al.: *Plasma Physics and Contrlled Nuclear Fusion Research 1990* (Washington, IAEA, 1990) Vol.2, p. 53
[13] Mazzucato E, Batha S H, Beer M, Bell M, Bell R E, Budny R V, Bush C, Hahm T S, Hammett G W, Levinton F M, Nazikian R, Park H, Rewoldt G, Schmidt G L, Synakowski E J, Tang W M, Taylor G and Zarnstorff M C: Phys. Rev. Lett. **77** (1996) 3145.
[14] Wong K-L, Bretz N L, Hahm T S and Synakowski E:: Phys. Lett. A **236** (1997) 339.
[15] Wong K-L, Itoh K, Itoh S-I, Fukuyama A and Yagi M: Phys. Lett. A **276** (2000) 281.
[16] See a review, e.g., Hahm T S: "Physics behind transport barrier theory and simulations" presented at 8th IAEA Technical Committee Meeting on H-mode Physics and Transport Barriers Physics (Toki, 2001) and to be published in Plasma Phys. Contr. Fusion **44** (2002)
[17] Krommes J A: Plasma Phys. Contr. Fusion **41** (1999) A641.
[18] Itoh S-I and Itoh K: J. Phys. Soc. Jpn. **68** (1999) 1891.
[19] Itoh S-I and Itoh K: J. Phys. Soc. Jpn. **68** (1999) 2611.
[20] Itoh S-I and Itoh K: J. Phys. Soc. Jpn. **69** (2000) 427.
[21] Itoh S-I and Itoh K: J. Phys. Soc. Jpn. **69** (2001) 408.
[22] Itoh S-I and Itoh K: J. Phys. Soc. Jpn. **69** (2001) 3253.
[23] Itoh K, Itoh S-I and Fukuyama A: Phys. Rev. Lett. **69** (1992) 1050.
[24] Yagi M, Itoh S-I, Itoh K, Fukuyama A and Azumi M: Phys. Plasmas **2** (1995) 4140.
[25] Uchida M, Fukuyama A, Itoh K, Itoh S-I, Yagi M: J. Plasma Fusion Res. SERIES, **2** (1999) 117.
[26] Yagi M: PhD thesis: *Study of anomalous transport based on drift and resistive i nstabilities in Heliotron/torsatron configuration* (Kyoto University, 1989).
[27] Itoh S-I, Itoh K, Zushi H, Fukuyama A: Plasma Phys. Contr. Fusion **40** (1998) 879.
[28] Itoh K, Itoh S-I, Fukuyama A, Sanuki H and Yagi M: Plasma Phys. Contr. Fusion **36** (1994) 123.

Recent Issues of NIFS Series

NIFS-704 S Toda and K Itoh
Theoretical Study of Structure of Electric Field in Helical Toroidal Plasmas
June 2001

NIFS-705 K Itoh and S-I. Itoh
Geometry Changes Transient Transport in Plasmas
June 2001

NIFS-706 M. Tanaka and A Yu Grosberg
Electrophoresis of Charge Inverted Macroion Complex: Molecular Dynamics Study
July 2001

NIFS-707 T-H Watanabe, H. Sugama and T Sato
A Nondissipative Simulation Method for the Drift Kinetic Equation
July 2001

NIFS-708 N. Ishihara and S. Kida
Dynamo Mechanism in a Rotating Spherical Shell Competition between Magnetic Field and Convection Vortices
July 2001

NIFS-709 LHD Experimental Group
Contributions to 28th European Physical Society Conference on Controlled Fusion and Plasma Physics (Madeira Tecnopolo, Funchal, Portugal, 18-22 June 2001) from LHD Experiment
July 2001

NIFS-710 V.Yu. Sergeev, R K Janev, M J Rakovic, S Zou, N Tamura, K V Khlopenkov and S. Sudo
Optimization of the Visible CXRS Measurements of TESPEL Diagnostics in LHD
Aug 2001

NIFS-711 M Bacal, M. Nishiura, M. Sasao, M. Wada, M Hamabe and H Yamaoka
Effect of Argon Additive in Negative Hydrogen Ion Sources
Aug 2001

NIFS-712 K. Saito, R Kumazawa, T. Mutoh, T Seki, T Watari, T. Yamamoto, Y Torii, N Takeuchi C. Zhang, Y. Zhao, A Fukuyama, F Shimpo, G. Nomura, M Yokota, A. Kato, M Sasao, M Isobe, A.V. Krasilnikov, T Ozaki, M. Osakabe, K Narihara, Y. Nagayama, S Inagaki, K Itoh, T Ido, S Morita, K. Ohkubo, M Sato, S. Kubo, T. Shimozuma, H Idei, Y Yoshimura, T. Notake, O Kaneko, Y. Takeiri, Y Oka, K. Tsumori, K. Ikeda, A. Komori, H Yamada, H Funaba, K Y. Watanabe, S. Sakakibara, R. Sakamoto, J. Miyazawa, K. Tanaka, B J. Peterson, N. Ashikawa, S. Murakami, T Minami, M. Shoji, S Ohdachi, S Yamamoto, H Suzuki, K Kawahata, M Emoto, H Nakanishi, N Inoue, N Ohyabu, Y Nakamura, S Masuzaki, S Muto, K Sato, T Morisaki, M Yokoyama, T Watanabe, M Goto, I. Yamada, K Ida, T Tokuzawa, N Noda, K Toi, S Yamaguchi, K. Akaishi, A. Sagara, K Nishimura, K Yamazaki, S. Sudo, Y Hamada, O. Motojima, M Fujiwara
A Study of High-Energy Ions Produced by ICRF Heating in LHD
Sep. 2001

NIFS-713 Y Matsumoto, S.-I Oikawa and T Watanabe
Field Line and Particle Orbit Analysis in the Periphery of the Large Helical Device
Sep 2001

NIFS-714 S Toda, M. Kawasaki, N. Kasuya, K Itoh, Y Takase, A. Furuya, M. Yagi and S -I. Itoh
Contributions to the 8th IAEA Technical Committee Meeting on H-Mode Physics and Transport Barriers (5-7 September 2001, Toki, Japan)
Oct. 2001

NIFS-715 A Maluckov, N. Nakajima, M. Okamoto, S Murakami and R Kanno
Statistical Properties of the Particle Radial Diffusion in a Radially Bounded Irregular Magnetic Field
Oct. 2001

NIFS-716 Boris V Kuteev
Kinetic Depletion Model for Pellet Ablation
Nov 2001

NIFS-717 Boris V. Kuteev and Lev D Tsendin
Analytical Model of Neutral Gas Shielding for Hydrogen Pellet Ablation
Nov. 2001

NIFS-718 Boris V Kuteev
Interaction of Cover and Target with Xenon Gas in the IFE-Reaction Chamber
Nov 2001

NIFS-719 A Yoshizawa, N. Yokoi, S.-I Itoh and K. Itoh
Mean-Field Theory and Self-Consistent Dynamo Modeling
Dec 2001

NIFS-720 V.N Tsytovich and K Watanabe
Universal Instability of Dust Ion-Sound Waves and Dust-Acoustic Waves
Jan. 2002

NIFS-721 V.N. Tsytovich
Collective Plasma Corrections to Thermonuclear Reactions Rates in Dense Plasmas
Jan 2002

NIFS-722 S. Toda and K. Itoh
Phase Diagram of Structure of Radial Electric Field in Helical Plasmas
Jan. 2002

NIFS-723 V.D. Pustovitov
Ideal and Conventional Feedback Systems for RWM Suppression
Jan 2002

NIFS-724 T Watanabe and H. Hojo
The Marginally Stable Pressure Profile and a Possibility toward High Beta Plasma Confinement in LHD
Feb. 2002

NIFS-725 S -I Itoh, K. Itoh, M Yagi, M Kawasaki and A Kitazawa
Transition in Multiple-scale lengths Turbulence in Plasmas
Feb 2002

NIFS-726 S -I Itoh, A Kitazawa, M Yagi and K Itoh
Bifurcation and Phase Diagram of Turbulence Constituted from Three Different Scale-length Modes
Apr 2002